Biofilm 6 (2023) 100157

Contents lists available at ScienceDirect

Biofilm

journal homepage: www.sciencedirect.com/journal/biofilm

Multiscale spatial segregation analysis in digital images of biofilms☆

Iztok Dogsa *, Ines Mandic-Mulec

Chair of Microbiology, Department of Microbiology, Biotechnical Faculty, University of Ljubljana, Večna pot 111, 1000, Ljubljana, EU, Slovenia

A B S T R A C T

Quantifying the degree of spatial segregation of two bacterial strains in mixed biofilms is an important topic in microbiology. Spatial segregation is dependent on spatial scale as two strains may appear to be well mixed if observed from a distance, but a closer look can reveal strong separation. Typically, this information is encoded in a digital image that represents the binary system, e.g., a microscopy image of a two species biofilm. To decode spatial segregation information, we have developed quantitative measures for evaluating the degree of the spatial scale-dependent segregation of two bacterial strains in a digital image. The constructed algorithm is based on the new segregation measures and overcomes drawbacks of existing approaches for biofilm segregation analysis. The new approach is implemented in a freely available software and was successfully applied to biofilms of two strains and bacterial suspensions for detection of the different spatial scale-dependent segregation levels.

1. Introduction

Two bacterial strains that are sharing an area could adopt two different states: they can either mix or segregate. Quantifying the segregation of different genotypes is highly relevant in population ecology [1] as microbial interactions typically take place within microscale cell aggregates [2]. In particular, organisms that exploit interspecific interactions to gain ecological advantage often co-aggregate [3]. Conversely, organisms that antagonize each other will tend to segregate in space, creating distinct micro-communities and increased diversity at larger spatial scales [4]. How an observer perceives this, while looking at a digital image, depends on the scale of observation, i.e. the field of view, which is the extent of the observable space that is seen by the observer at any given moment. For example, two bacterial strains, forming a mixed biofilm, can be well separated in the small spatial scales (observed when zooming in to the image, to the small field of view of, e.g. 30 μm × 30 μm), forming small patches, but the patches themselves can appear well mixed (observed when zooming out, to the large field of view of, e.g. 300 μm × 300 μm). This opens a dilemma if such a biofilm is well mixed or rather segregated. It is therefore important to have an approach that can analyse, and consider spatial segregation at different spatial scales and calibrate calculated segregation values in relation to the positive and negative controls (minimum and maximum segregation extremes). Moreover, the species-specific labelling techniques, such as FISH, or fluorescence protein labelling coupled with fluorescence microscopy, which opened the doors into visualization of mixed microbial communities and consequences of their interactions [5–9] call for quantitative evaluation of genotype's segregation levels. The digitalization of modern image acquisition equipment makes it possible to acquire large-field-of-view, high-resolution 3D images, underlining the need for data reduction and fast analysis [10]. Currently available biofilm analysis software, such as BiofilmQ [11] or COMSTAT [12] do not include biofilm segregation analysis. Therefore, it is not surprising that the segregation in biofilms is sometimes only qualitatively assessed [13]. To tackle this gap we developed new multiscale spatial segregation (*MSSegregation*) analysis approach, which we applied to quantify the segregation and spatial mixing of genetically different or identical *Bacillus subtilis* strains in a floating biofilm [14]. In this article we provide the detailed explanation of the upgraded method, its validation, the publicly available free *MSSegregation* analysis software and additional examples of strains segregation analysis to make the novel method more accessible to the user.

2. Results

2.1. Existing methods for biofilm segregation analysis in digital images

Before developing new segregation metrics, we reviewed the established ones and their potential to consider spatial scale dependant segregation. The first group of methods extracts the segregation information by scanning the 2D space in a digital image by 1D subunits. For

☆ Given her role as a member of the Editorial board, Ines Mandic-Mules was not involved in the peer review of this article and had no access to information regarding its peer review.

* Corresponding author.
E-mail address: iztok.dogsa@bf.uni-lj.si (I. Dogsa).

https://doi.org/10.1016/j.bioflm.2023.100157
Received 23 March 2023; Received in revised form 15 September 2023; Accepted 19 September 2023
Available online 20 September 2023

example, the intermixing index represents the average number of colour changes along microbial community height [15] or along the perimeter of the circle of certain radius placed over the colony depicted in digital image [16]. The inability of 1D segregation analysis methods to capture the segregation information in the second dimension can be overcome by employing the methods that evaluate the strain composition in 2D subunits. By the method deployed by Mitri et al. [17] and Nadell et al. [18] the segregation index was computed as the mean value of the relative frequency of strain 1 across the population of focal cells of the strain 1 within 10 cell distances. The cells of strain 2 were treated as empty space. The method reveals accurately segregation level as long as there is no empty space in the biofilm image and the overall ratio of the cells of the two strains is 1:1. This is, however, often not true, for example, even the strains of the same species can form biofilms with profoundly different ratios [14]. Moreover, biofilms are spatially structured, often containing areas with no cells [19], forming channels visible on microscopy images [20]. Another segregation metric for digital image analysis that considers segregation of strain 1 and strain 2 was published by van Gestel et al. [21], who addressed the above problems:

$$S_{VG} = \left[\frac{1}{n}\sum_{i=1}^{n}\frac{a}{a+b}\right]_a - \left[\frac{1}{n}\sum_{i=1}^{n}\frac{a}{a+b}\right]_b \quad \text{(eq 1)}$$

Here, a and b are areas covered by pixels corresponding to the strain 1 and strain 2 frequencies within a chosen radius surrounding a focal cell. First term on the right-hand side corresponds to the average relative frequency of strain 1 around focal cell of strain 1 and second term is the average relative frequency of the strain 1 around focal cell of strain 2; n is the number of randomly sampled areas of chosen radius in the analysed image. The equation addresses which scenario is more likely: the strain 1 gathers around strain 1 or the strain 1 gathers around strain 2. If the two likely-hoods are the same, the strain 1 equally prefers strain 1 and 2. In this case the difference of the two terms in eq (1) is 0, i.e. $S_{VG} = 0$, meaning no segregation. On the other hand, if strain 1 prefers strain 1 to strain 2, $S_{VG} > 0$ and in the fully segregated case, $S_{VG} = 1$. By changing the radius around the focal cell, it is possible to obtain S_{VG} at different spatial scales. Therefore, the eq (1) appears to be a good basis to construct a segregation measure that takes dependency of segregation on different spatial scales into account. However, it has few important drawbacks. The local cell densities in the native biofilms can vary, but the less dense regions in the same digital image contribute equally to the averages in eq (1) as high dense regions, although the biomass compared

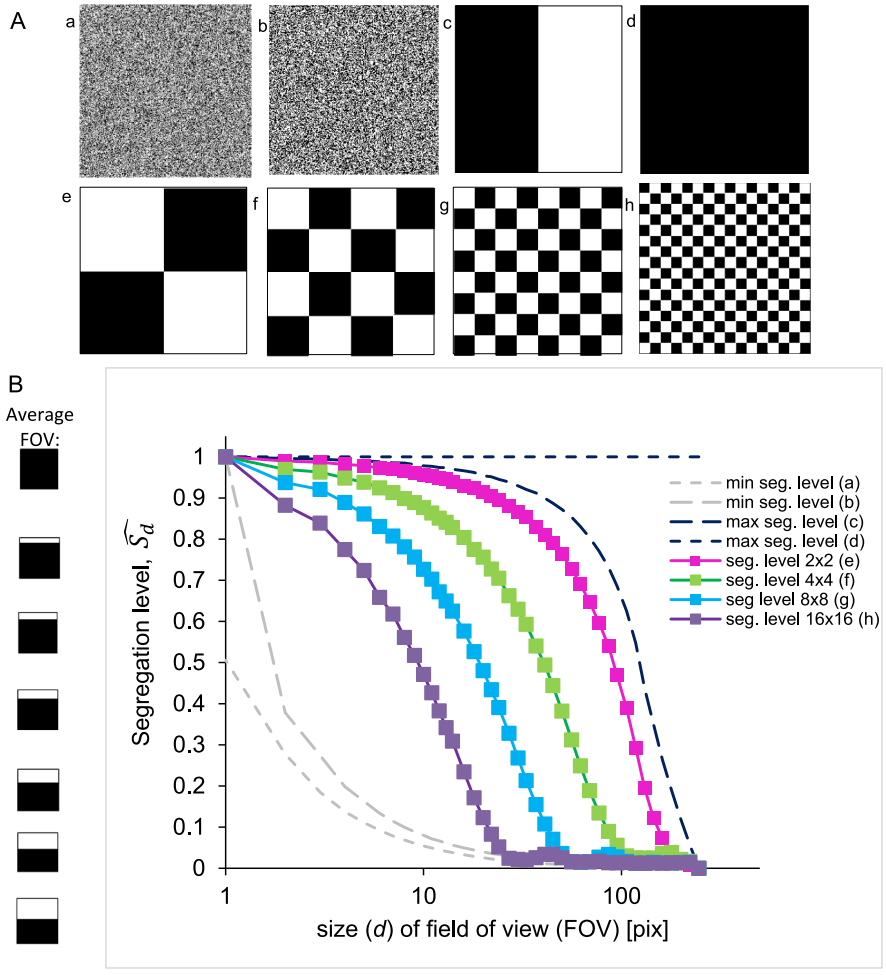

Fig. 1. The segregation analysis of pixel-sized black and white particles. In (A) half of the 246 × 246 pixel images are black pixel-sized particles and half are white pixel-sized particles; (a) and (b) show two types of minimal segregation i.e. the best possible mixing: in (b) pixel particles cannot overlap and in (a) overlapping is allowed; (c) and (d) correspond to two types of maximal segregation among black and white particles. In (c) they are maximally separated, but present in the space; in (d) black particles fully displaced white particles; (e)–(h) chessboard examples of segregated black and white pixels. The images in panel (A) were analysed by our algorithm based on eqs (5)–(11)) and corresponding segregation levels as a function of size of field of view (FOV) are given in panel (B). The numerical segregation levels (y-axis) are graphically represented by Average FOV as determined by eq (6); $\widehat{S_d} = 0$ both type of particles are present, $\widehat{S_d} = 1$, only one type of particle is present in the FOV. The sampling error of algorithm estimated by eq S2 is within the symbol size.

is not the same. Also, the two terms in eq (1) are obtained independently and their averages are finally subtracted. In this process the information about local correlations between the two strains is lost. Moreover, it is difficult, if not impossible, to decode the value of S_{VG} to the expected ratio of the two strains at certain size scale, which is an important quantity in many ecological simulations. Because the reference point to put the calculated S_{VG} in a perspective is missing, it is difficult to make relative comparisons among different S_{VG}. For all $0 < S_{VG} < 1$ one can only conclude that S_{VG} values are somewhere between randomly mixed sample ($S_{VG} = 0$) and fully segregated sample ($S_{VG} = 1$). However, even this may not be always true. We tested the algorithm based on eq (1) on image (c) in Fig. 1A, which depicts maximally segregated black and white particles of pixel size. The obtained calculations showed that at size scales much smaller than the image size (246 pix x 246 pix), S_{VG} approaches the expected value of 1 (at $r = 5$ pix $S_{VG} = 0.99 \pm 0.01$), but at larger size scales that are however still much smaller than the image size, S_{VG} significantly deviates from the expected value of 1 (at $r = 50$ pix $S_{VG} = 0.71 \pm 0.01$). Testing image (b) in Fig. 1A, which depicts minimally segregated black and white pixels gave a similar, albeit less pronounced problem. At size scales much larger than the pixel sized particle size, the S_{VG} is at the expected value of 0 (at $r = 50$ pix $S_{VG} = 0.00 \pm 0.01$), but at size scales approaching the pixel size, i.e. looking at neighbouring bacteria cells, the value of S_{VG} deviates again from 0 (at $r = 1.5$ pix $S_{VG} = 0.11 \pm 0.01$). Due to the described drawbacks, we decided to developed different segregation metrics on which we based multiscale spatial segregation analysis.

Briefly, our approach is based on calculating the segregation level in the square shaped field of view (FOV) of size d that is randomly placed over a digital image. The idea came from microscopy, where an observer can change the size of FOV by changing magnification and by moving microscopy stage in x and y direction changing the position of FOV.

2.2. Derivation of segregation measures for multiscale spatial segregation analysis

In this section, we will use simple binary images (Fig. 1A, (a) and (d)) depicting cases of minimal and maximal segregation to assist the derivation of segregation measures. These images represent the 2D space of much bigger size than the size of the two types of particles occupying the 2D space. In Fig. 1A, (a)–(d) the particles are of pixel size. In this system, we define complete segregation as the total absence of one type of particle on account of the presence of another type of particle in an arbitrary region in an image. The region could be of any shape, but for the sake of simplicity, we chose a square with side length d that we call the "field of view" (FOV) of size d. This minimal size ($dmin$) may represent the size of a pixel in an image or be as big as whole image ($dmax$). The examples of segregation extremes are shown Fig. 1A. The segregation is minimal in image (a) (Fig. 1A), where equal parts of white and black particles of pixel size were randomly mixed and the sharing of the same area was allowed. On average, both particles are present in the FOV in equal portions. The measure sought for segregation should in this case display the minimum value. In contrast, the segregation is maximal in the image (d), (Fig. 1A), where pixel-sized particles have totally displaced the white particles. Therefore, in this image, regardless of the scale of observation (for all FOVs of $dmin \leq d \leq dmax$), only one type of the particle is present in the FOV. The segregation measure we would like to derive should in this case display maximum value for all d. Regardless of the segregation case discussed, the segregation measure should evaluate the presence or exclusion of both types of particles in the FOV.

In a digital image, the size of an area under consideration is defined as number of pixels that comprise the considered area. The smallest unit of area is thus 1 pixel and objects smallest than 1 pixel are not visible. If the particles are approximately of the same size (e.g. bacterial cells) the number of particles in the field of view (FOV) is proportional to the area they occupy. Let us say that the two types of particles occupy the areas with size a and b, respectively. We can measure the degree of particle exclusion in the FOV by the absolute difference of a and b. The significance of an absolute difference depends on the total area of particles ($a + b$) in the FOV; therefore, the relative difference is a better measure for segregation. This simple segregation measure in the FOV of size d can be given as:

$$s_d = \frac{|a-b|}{a+b} \quad \text{(eq 2)}$$

The s_d is 0 if both particles are present in the FOV in equal portions and 1 if only one type of particle is present. However, this simple segregation measure assumes that the two types of particles in an entire digital image are present in equal amounts (i.e. in overall ratio of 1:1), but this is often not true. This is important, because if one type of particle is more common in a whole image than it is more likely that the same particle type will be also dominant in smaller region of the image (i.e. in the FOV) and this does not necessarily indicate high segregation. In order to ensure the validity of eq (2) for any particle ratio, it is necessary to normalize the size of area of particles in the FOV to the size of total area of the two types of particles in a whole image, denoted as A and B, respectively. In this way we obtain local segregation level defined as:

$$S_d = \frac{|a/A - b/B|}{a/A + b/B} \quad \text{(eq 3)}$$

If we move randomly n times over an image with a FOV of size d and calculate the local segregation level by eq (3) for i-th FOV (denoted as $S_{d,i}$ in eq (4)), we obtain the arithmetic mean segregation level of the FOV of size d, denoted as $\overline{S_d}$:

$$\overline{S_d} = \frac{1}{n}\sum_{i=1}^{n} S_{d,i} \quad \text{(eq 4)}$$

In a digital image such as a microscopy image, the entire area is not always occupied by particles. Hence, some FOVs might contain low number of particles or even be empty, while others may contain high number of particles. Therefore, we propose that it is better to replace the arithmetic mean segregation level, $\overline{S_d}$, as a segregation measure with the weighted mean segregation level, $\widehat{S_d}$, where weights, $w_{d,i}$, are the total normalized areas of particles ($a_i/A + b_i/B$) in the FOV of size d:

$$\widehat{S_d} = \frac{\sum_{i=1}^{n} S_{d,i}\, w_{d,i}}{\sum_{i=1}^{n} w_{d,i}} \quad \text{(eq 5)}$$

The segregation level, $\widehat{S_d}$, will be 1 if only one type of particle is present in the FOVs, and 0 if both types of the particles are present in equal amounts normalized to the total amount of each particle in the image (i.e. $|a/A - b/B| = 0$ in eq (3)). Note that if the FOV is empty, its weight $w_{d,i} = 0$ and therefore empty FOV do not contribute to the average.

To aid the interpretation of the segregation level, it will be useful to obtain the typical ratio of the two types of particles in the FOV of size d. For example, in a microscopy image of a biofilm composed of two strains with an overall ratio of A:B (as determined from whole image), we would like to know what is the strain ratio in the FOV of d if the segregation level is $\widehat{S_d}$. One can easily envision how the FOVs with $\widehat{S_d} = 0$ or 1 look-like. In case of $\widehat{S_d} = 0$, which means no segregation is present, the strains in the FOVs will be in the ratio that one expects from their total areas (i.e. a:$b = A$:B); in the case $\widehat{S_d} = 1$, which means maximal segregation is present, only one of the two strains will be present in the FOV. It is less straightforward to determine the strain ratio in the cases with $\widehat{S_d}$ between the extreme values of $\widehat{S_d}$. For example, what is the strain ratio in the case of $\widehat{S_d} = 0.5$ compared to the ratio in more segregated biofilm at $\widehat{S_d} = 0.6$? Let us say that we want to express

the ratio of the two strains from the point of perspective of more (or equally) abundant strain (as determined from whole image) in the biofilm. In this case the ratio of the two strains in the whole image can be expressed as X:1 (with $X \geq 1$), where X corresponds to more (or equally) abundant strain. In the FOV of size d the corresponding areas of the strains are, a', for more (or equally) abundant strain and area b' for the less (or equally) abundant strain. Assuming that $\widehat{S_d}$ (which is weighted average of S_d, eq (5)) represents well a typical segregation level in the biofilm in the FOV of size d, we can rearrange the eq (3) to the useful relation:

$$\frac{a'}{b'} = X\frac{(1+\widehat{S_d})}{(1-\widehat{S_d})} \quad \text{(eq 6)}$$

It means that at segregation level $\widehat{S_d}$ present in the FOV of size d, with the more abundant strain being X-times more abundant than the other strain in the whole image, we can expect the ratio of the two strains to be a': b'. Note that the areas in eq (3) are not fixed by their dominance, therefore we used for corresponding areas different symbols in eq (6). For above example, when the total abundancies of the two strains in the biofilm are 1:1 (i.e. X = 1), we get that the strain ratio is 3 : 1 at $\widehat{S_d} = 0.5$, and the strain ratio is 4:1 at $\widehat{S_d} = 0.6$, which is ecologically relevant difference. The eq (6) can be also interpreted in this way-as the X:1 is the ratio of the overall strain abundance (in the whole image), one would expect that the same ratio is going to be observed in the considered FOV of size d, if no segregation is present. The term $(1+\widehat{S_d})/(1-\widehat{S_d})$ is telling us what will be the change in the expected strain ratio if the segregation level is $\widehat{S_d}$. If no segregation is present (i.e. $\widehat{S_d} = 0$) the ratio in the FOV is just the same as expected ratio (i.e. X:1). For any other segregation level (i.e. $0 < \widehat{S_d} < 1$) the ratio in the FOV (a': b') will be increased.

By calculating the segregation level, $\widehat{S_d}$, at different d of FOV (sizes of the field of view), one can obtain a graph of the segregation level versus the FOV size of a particular image (segregation level curves). The segregation level curves can be then compared among several binary systems (e.g. two or more biofilms, each composed of two different strains). In this way it is possible to compare segregation level at different sizes of FOV among several binary systems, because the differences in segregation level among different binary systems can vary significantly with the size of FOV. Although this approach gives a very good insight into different segregation patterns, sometimes a simpler presentation of segregation is sufficient and can be a more convenient form of data to use in a subsequent presentation or analysis. For example, in an experiment where two different bacterial cultures are mixed and their segregation is followed over time under the microscope, it may be useful to express segregation level versus time in a simple 2D plot. In such cases d, the size of FOV might be redundant. On the other hand, the difference among segregation level curves can be dependent on d. For example, from large distance the two images of two mixed biofilms may appear equally well segregated, but closer inspection reveals that one biofilm is more segregated than the other. For such cases, the segregation in an image described by single number that takes into account segregation levels at several distances is required. To obtain this, we propose to average segregation level, $\widehat{S_d}$, over all d to give a distance-averaged segregation level, which we call the multiscale spatial segregation level, *MSSL*:

$$MSSL = \frac{1}{dmax - dmin}\int_{dmin}^{dmax} \widehat{S_d}\, \mathrm{d}(d) \quad \text{(eq 7)}$$

The *MSSL* represents an average segregation level that is hypothetically obtained in the FOV of sizes $dmin \leq d \leq dmax$. In this article the *dmin* and *dmax* always refer to the full range of FOV sizes shown in the plots, but in principle one could calculate *MSSL* also in the narrower range.

The extremes of $\widehat{S_d}$ (e.g., for (a) and (d) in Fig. 1A), denoted as $\widehat{S_d^{min}}$ and $\widehat{S_d^{max}}$, give $MSSL_{min}$ and $MSSL_{max}$, respectively:

$$MSSL_{min} = \frac{1}{dmax - dmin}\int_{dmin}^{dmax} \widehat{S_d^{min}}\, \mathrm{d}(d) \quad \text{(eq 8)}$$

$$MSSL_{max} = \frac{1}{dmax - dmin}\int_{dmin}^{dmax} \widehat{S_d^{max}}\, \mathrm{d}(d) \quad \text{(eq 9)}$$

The values of $\widehat{S_d^{min}}$ and $\widehat{S_d^{max}}$ are important as they represent segregation negative and positive control, respectively. For example, if $\widehat{S_d} > \widehat{S_d^{min}}$, it means that the segregation at the spatial scale of d is higher than the segregation in a randomly mixed system, and if $\widehat{S_d} = \widehat{S_d^{max}}$, it means that segregation has reached the maximum possible segregation at spatial scale of d in a given system. Accordingly, $MSSL_{max}$ represents the maximal multiscale spatial segregation level and $MSSL_{min}$ the minimal spatial segregation level. To take this into account, the *MSSL* in eq (7) has to be compared to $MSSL_{min}$ and normalized on the range of *MSSL*, which gives a version of *MSSL*, relative *MSSL* (*rMSSL*), corrected by segregation extremes:

$$rMSSL = \frac{MSSL - MSSL_{min}}{MSSL_{max} - MSSL_{min}} \quad \text{(eq 10)}$$

The corrections assure that if there is no segregation in the system, $rMSSL = 0$ and if the segregation is at maximum, $rMSSL = 1$.

Ideally, the segregation level, $\widehat{S_d^{max}}$ and $\widehat{S_d^{min}}$ will be for all FOVs of $dmin \leq d \leq dmax$ 1 and 0, respectively. This gives $MSSL_{max} = 1$ and $MSSL_{min} = 0$; this is, however, possible only if the opposite particles either fully displace each other or always share the same pixels. In this case, *rMSSL* in eq (10) becomes equal to the uncorrected variant, *MSSL* in eq (7). To obtain $\widehat{S_d^{max}}$ and $\widehat{S_d^{min}}$, the *MSSsegregation* first constructs synthetic binary images (via simulation) displaying the maximum and minimum segregation cases and then calculates segregation levels (Fig. S2). For the uncertainty estimation and application of multiscale spatial segregation analysis on 3D images, the reader is referred to the Supplementary (SI Results, The uncertainty in multiscale spatial

Segregation analysis, Multiscale spatial segregation analysis in 3D digital images).

Another interesting measure that could be inferred from $\widehat{S_d}$ as a function of d is a multiscale spatial segregation distance (*MSSD*), which we define as:

$$MSSD = \frac{1}{Smax}\int_{dmin}^{dmax} \widehat{S_d}\, \mathrm{d}(d) \quad \text{(eq 11)}$$

where $Smax = 1$, regardless of the distance. By the division of the integral by *Smax* one obtains a distance. This distance can be interpreted as the distance over which $\widehat{S_d} = 1$ (i.e. maximal segregation level), if we theoretically compact all segregation levels, $\widehat{S_d}$, from *dmin* to *dmax* to the distances from *dmin* to *MSSD*. In the hypothetical image where the overall abundance of the two particles is equal, the *MSSD* approximately matches the size of homogenous hypothetical aggregates (patches composed of only one type of the particle) distributed without any gaps between them. These aggregates may contain either one type of particle or the other, but not both of them. For samples with higher level of segregation, one expects larger aggregates composed of only one type of particles. A good example are the chessboards in Fig. 1 with corresponding *MSSD* listed in Table S1. Note that calculated *MSSD* are slightly lower than true size of the squares, which is because some of the randomly placed FOVs with $d > 1$ pix contain both types of particles, i.e. have $Sd < 1$, thereby decreasing $\widehat{S_d}$ (eq (5)) and hence *MSSD* (eq (11)).

Equations (7)–(11) are dependent on the choice of *dmin* and *dmax*. Idealy, *dmax* would extend into infinity, but in praxis it has to be limited to the maximal size of FOV, which is usually the size of the investigated image. On the other hand, the choice of *dmin* that signifies the smallest

size of FOV where the segregation levels are evaluated, should be such that the optical information in the FOV will predominantly come from x, y plane and that it will not go below the resolution of microscope in x,y plane. This means in 2D images of thin microscope specimens, where the bacteria are in single layer *dmin* should not go below the optics resolution. In thick specimens the situation is more complicated. Firstly, because it can happen that the sample is too thick, and deepest layers of the biofilm cannot be optically accessed and secondly, all of the collected information in the 2D FOV contains not only information coming from x,y plane of the biofilm, but also some information coming from z-axis. In this case it is advisable to use confocal microscope or similar, to reduce out of plane light. However, even in this case, due to the intrinsic imperfection of the confocal systems the light in the confocal 2D image does not come from perfectly thin optical slice. This slice has some finite thickness, usually referred to as optical slice thickness. Therefore, if $\widehat{S_d}$ is not to be dominated by segregation in the z-axis, we suggest that *dmin* should not go below optical slice thickness (see Supplementary information, Multiscale spatial segregation analysis in 3D digital images for more details). Otherwise, the interpretation of $\widehat{S_d}$ as a function of size *d* of FOV will become more complicated. In the case the thick samples are observed with non-confocal system, the optical slice thickness cannot be defined and in the FOV light from several planes will be collected, which makes the interpretation of the results more difficult. Without any knowledge on how light from different planes contributes to the observed image, one can still say that limiting *dmin* to specimen thickness should assure that $\widehat{S_d}$ will not become dominated by segregation in z-direction. Nevertheless, in all thick specimens the evaluation of areas of particles will have some errors, because of the 2D projections of finite volumes of observed optical slices. However, as long as the errors are equally affecting both particles the segregation levels as determined by eq (3) should not be greatly affected. For example, if *a* and *A* or *b* and *B* are both equally inflated, the $\widehat{S_d}$ does not change.

When utilizing an imaging device with limited resolution and a detection threshold to observe systems comprised of small particles (e.g., when observing weakly fluorescent bacteria with a typical stereomicroscope), additional challenges may emerge. The estimation of particle counts within the field of view (FOV) may result in either underestimation or overestimation. When these deviations occur in opposite directions for the two types of particles, it can have a substantial impact on the accuracy of $\widehat{S_d}$. For example, the observed patch in the biofilm can appear as being comprised of red bacteria only, although the green bacteria are present. However, they may go undetected due to their lower quantity and dispersion within the same cluster. At the same time, there is a possibility of overestimating the count of red bacteria, as the imaging device's limited resolution may not capture empty spaces effectively. Therefore, unless the assumption that most of the bacteria in the clusters are visible to the imaging device and that the bacterial density at size scales below the resolution limit of the imaging system is the same in most of the clusters throughout the FOV can be made, the segregation analysis shall not be performed.

We implemented our approach in *MSSegregation* analysis software (for details see Methods, Macro implementation), the workflow of analysis is depicted in Fig. S2. The main output parameters (based on eq (3) to eq (11)) of the segregation analysis and their brief description are summarized in Table 1. For advanced users, the auxiliary segregation measures and statistics (based on eqs S4 to S6) are also calculated by the software.

2.3. Validating multiscale spatial segregation analysis by application to synthetic images

To validate the multiscale spatial segregation analysis, eqs (5)–(11) were implemented in an algorithm encoded in the imageJ Macro language (see Methods, Macro Implementation) and applied to synthetic images (Fig. 1A) with an easy-to-predict outcome. The black pixel-sized particles completely excluded the white pixel-sized particles from space of the image [(Fig. 1A), (d)]. As expected in Section 2.1., one can observe in Fig. 1B the segregation level, $\widehat{S_d} = 1$, regardless of the spatial scale of the observation (*d* of FOV). On the other hand, in a case where none of the particles can exit the system, the segregation maximum will have a different appearance (Fig. 1A), (c). Here, white and black pixel-sized particles coexist at the spatial scale of the whole image (i.e., when the FOV is of *dmax*) and both types of particles are present in equal (relative) numbers. Correspondingly, the $\widehat{S_d}$ at $dmax = 0$ (Fig. 1B). However, when we turn to smaller spatial scales (smaller *d* of FOV), one of the two type of particles becomes quickly dominant and, as expected, segregation increases rapidly. Very soon, FOVs containing only one type of particle become dominant and segregation at this spatial scale has to approach 1, as can indeed be observed in Fig. 1B. On the contrary, the segregation level has to be significantly lower in Fig. 1A (b), where image (c) was pixel randomized and overlapping of opposite pixels was not allowed. Here, as predicted, the segregation level, $\widehat{S_d}$, is close to zero for all *d* (FOV sizes), except for *d* approaching particle size (pixel in this case), where $\widehat{S_d}$ rapidly increases to 1 (Fig. 1B). When overlapping is permitted, as is the case in image (a), the $\widehat{S_d}$ correctly drops further than is the case in image (b). At $d = 1$, where the size of the FOV is 1×1 pixel, half of the FOV contains either black or white pixel particle ($S_d = 1$) and

Table 1
Main output parameters of segregation analysis by *MSSegration* package running in Fiji-ImageJ.

Output parameter	The name in *MSSegregation* software	Brief description
$\widehat{S_d}$ vs *d*	segregation level in your image (Sd^)	Shows how weighted mean segregation level (eq (5)) varies with the size *d* of field of view (FOV) in the sample image (e.g. microscopy image of the biofilm).
$\widehat{S_d^{min}}$ vs *d*	segregation level in min seg image (Sd^min)	Shows how weighted mean segregation level varies with the size *d* of field of view (FOV) in the simulated minimum segregation case image.
$\widehat{S_d^{max}}$ vs *d*	segregation level in min seg image (Sd^max)	Shows how weighted mean segregation level varies with the size *d* of field of view (FOV) in the simulated maximum segregation case image.
X:1	ratio of the two types of particles	Tells what is the overall ratio (in the whole image or stack of images) between the two types of particles.
Sd vs x,y	local Sd (unweighted) together with coordinates	Shows how local segregation level (eq (3)) in the FOV of size *d* varies across the sample image.
MSSL	multiscale spatial segregation level (MSSL), your image	A single value quantity (eq (7)) that is an average of $\widehat{S_d}$ over all *d* for the sample image.
$MSSL_{min}$	multiscale spatial segregation level (MSSL), min image	A single value quantity (eq (8)) that is an average of $\widehat{S_d}$ over all *d* the simulated minimum segregation case image.
$MSSL_{max}$	multiscale spatial segregation level (MSSL), max image	A single value quantity (eq (9)) that is an average of $\widehat{S_d}$ over all *d* for the simulated maximum segregation case image.
rMSSL	relative multiscale spatial segregation level (rMSSL-your image)	A single value quantity that gives *MSSL* relative to $MSSL_{min}$ and $MSSL_{max}$; it runs from 0 to 1 (eq (10)).
MSSD	multiscale spatial segregation distance (MSSD)	A single value quantity (eq (11)) that gives an idea of the size of hypothetical aggregates composed of only one type of particle in the sample image.

half of the FOV contains black and white pixel particle ($S_d = 0$), giving the predicted segregation level, $\widehat{S_d} = 0.5$ (Fig. 1B). The challenging tests are more complex chessboard images of (e)–(h) in Fig. 1A. As can be seen in the graph in Fig. 1B, our approach correctly predicts the chessboard segregation levels, $\widehat{S_d}$; with smaller chessboard squares, the size of the FOV, where $\widehat{S_d}$ of pixel-sized particles starts to rapidly increase, decreases. Accordingly, the *MSSL*, (eq (7)), which is the size of the FOV-averaged segregation level, decreases in the direction of the decreasing size of the chessboard squares (Table S1). As the chessboard squares consist of several basic pixel-sized particles that are clustered together, the *MSSL* does not reach the *MSSL* value for the minimal segregation case. Also, the *MSSL* of the maximal segregation case is not reached, because in image (e), i.e., the 2 × 2 chessboard, the mixing is still better than in the case of image (c), where pixel-sized particles minimized contacts in order to avoid each other. The relative *MSSL* (eq (10)), which takes explicitly into account the maximum and minimum segregation cases and is denoted *rMSSL* (Table S1), tells us what the multiscale segregation level is on a scale from 0 to 1. As expected, the segregation in the 2 × 2 chessboard with $rMSSL = 0.72 \pm 0.05$ is relatively close to the maximum segregation, where the black and white pixel particles are not allowed to exclude each other from the space (image (c) in Fig. 1B). Doubling the number of chessboard squares roughly halves the *rMSSL*. Also, as expected, *MSSD* (eq (11)), which corresponds roughly to the size of single square, halves by doubling the number of chessboard squares. Overall, the proposed multiscale spatial segregation analysis based on eq (5) to eq (11) gave the expected results.

To further validate the new approach, we have applied it to the actual cases of segregation. The first case was a real-life scene with a predictable multiscale segregation analysis outcome and is given in Supplementary, SI Results, Mixing of oats and raisins, Fig. S1. The results were entirely consistent with our expectations, showing that increased mixing of oats and raisins resulted in reduced segregation levels. Therefore, we went on testing the biologically relevant cases given in the next sections.

2.4. Biofilms of two bacterial strains

The evaluation of cell segregation in biofilms composed of two fluorescently labelled bacterial strains by visual observation alone represents a challenge (Fig. 2A). First, the segregation level may change with the scale of observation, i.e. with the size of field of view (FOV), as for example in Fig. 1B. Second, a biofilm confocal image typically comprises

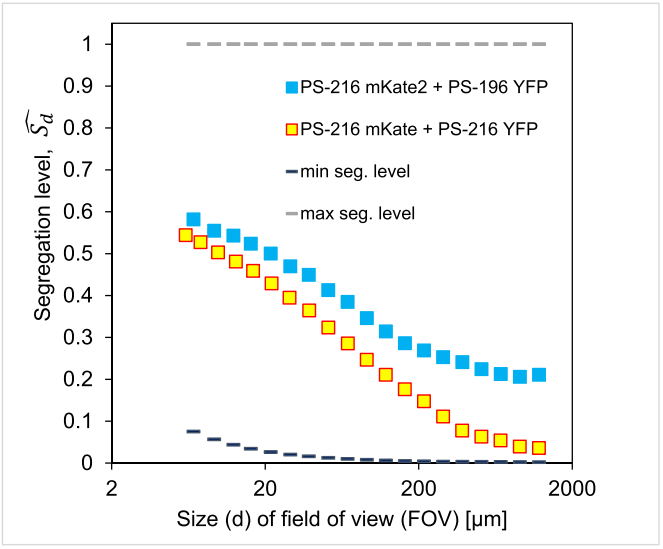

Fig. 2B. The CLSM images of *B. subtilis* biofilms in Fig. 2A were analysed by our algorithm based on eqs (5)–(11) and corresponding segregation levels as a function of size of field of view (FOV) are presented for all bacterial strain combinations. The curves of simulated minimal and maximal segregation cases for the two bacterial strain combinations do not differ significantly, therefore only one max and min segregation curve is presented. The sampling error is within the symbol size. The curves shown represent one of the three replicates shown as averages in Supplementary information of [14].

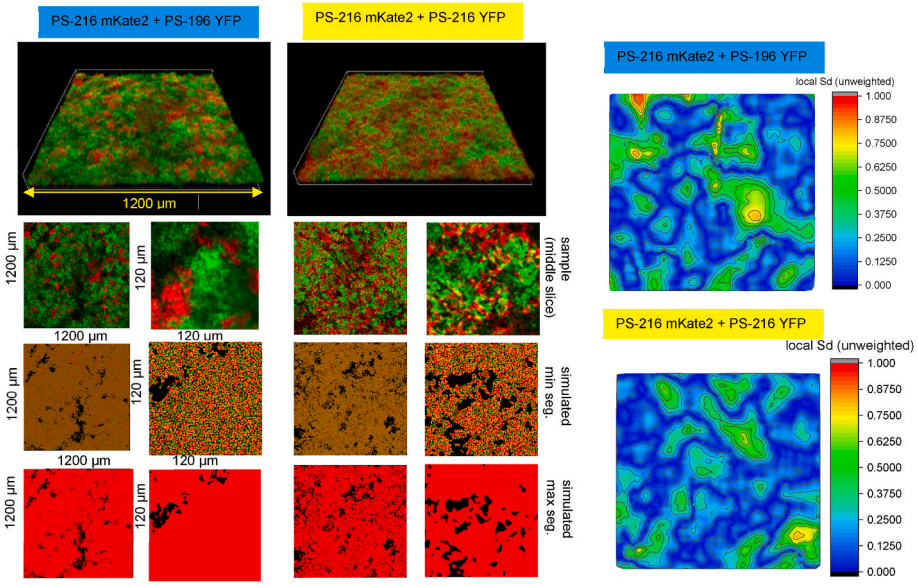

Fig. 2A. Multiscale spatial segregation analysis of two strain biofilms, example 1. 3D reconstructions presented as maximum intensity projections of biofilms formed by two differently labelled bacterial strains based on confocal scanning laser microscopy (CLSM) image slices are shown on top. The green and red color represents *B. subtilis* strain constitutively expressing YFP and mKate fluorescent protein, respectively. 15-25 image slices (forming a CLSM stack of image slices) with optical slice thickness of 14 μm were acquired for each biofilm. The middle image slice in the CLSM image stack representing the FOVs of size (*d*) of 1200 μm x 1200 is shown together with additional zoom in (120 μm x 120 μm). The corresponding image of simulated minimal and maximal segregation of the two strains in the biofilm is shown. For simulation of maximal segregation, we assumed that only one strain is present in the slice of CLSM stack (in this case the red, mKate strain, but result would be the same for yfp strain). The contour plots show local segregation level S_d at $d = 120$ μm in the space of the middle slice (1200 μm x 1200 μm).

of 15–25 image slices and the cell distribution can vary from slice to slice. We compared here simulated minimal and maximal segregations to segregations in experimental microscopic images (Fig. 2A) of floating biofilms composed of two bacterial strains labelled with either Yellow fluorescent protein (YFP) or Red fluorescent protein (mKate2). Visual inspection of the two images suggests that the strains are neither entirely segregated nor perfectly mixed (Fig. 2A), but without multiscale spatial segregation analysis (of all image slices), no quantitative descriptor of segregation can be given. Therefore, for example, it is not possible to determine which of the two biofilms is more segregated. Performing multiscale spatial segregation analysis gives a higher *rMSSL* value for the strain pair PS-216 mKate2 + PS-196 YFP compared to PS-216 YFP + PS-216 mKate2, meaning the segregation is stronger in the first pair (Table S3) and comparable to the value obtained by mixing oats and raisins at t3 (Fig. S1, Table S2). At t3, oats and resins were mixed, but have not yet reached maximal mixing, i.e., $rMSSL = 0$. If the two biofilms were to be interpreted in the terms of hypothetical patch sizes belonging exclusively to one of the two strains, the patches of PS-216 mKate2 + PS-196 YFP would be at $MSSD = (300 \pm 10)$ μm, which is larger than the patches of PS-216 YFP + PS-216 mKate $MSSD = (150 \pm 10)$ μm. One of the advantages of our approach is also that we can spatially assign the segregation levels, as shown in contour plots (Fig. 2A). The local segregation levels, as determined by eq (3) in the FOV of size $d = 120$ μm were positioned in the plot according to the coordinates of the centre of the many FOVs randomly placed over the image (slice). In the analysed example slice, it can be seen that segregation has patchy distribution in both strain pairs, but the values are higher in strain pair PS-216 mKate2 + PS-196 YFP, indicating that at $d = 120$ μm the average segregation is stronger in this strain pair. As can be seen in Fig. 2B, the latter holds for all the sizes of FOV. As expected, the segregation in both biofilms is high at small d and decreases towards higher d. At the smallest observable FOV of size corresponding to a few bacteria ($dmin = 7$ μm), the biofilms PS-216 mKate2 + PS-196 YFP and PS-216 YFP + PS-216 mKate2 have $\widehat{S_d} = 0.58$ and 0.53, respectively. This indicates a high segregation level as most FOVs will have high dominance of one of the two strains in the biofilm and that the neighbouring cells will be most likely of the same strain. Although the segregation level and strain ratio in both biofilms is similar at small d (according to eq (6), with X = 1, the strain ratio in PS-216 mKate2 + PS-196 YFP is 3.8:1 and in PS-216 YFP + PS-216 mKate2 is 3.3 : 1, for a simplified graphical interpretation of $\widehat{S_d}$, see y-axis of Fig. 1B) the difference in segregation level grows with d (slopes of $\widehat{S_d}$ curves of both biofilms are correspondingly different, Table S3). For example, at $d = 500$ μm the biofilms PS-216 mKate2 + PS-196 YFP and PS-216 YFP + PS-216 mKate2 have $\widehat{S_d} = 0.22$ and 0.06 (corresponding to the ratios of 1.6 : 1 and 1.1 : 1), respectively.

We next compared two mixed biofilms where the distinction between the two segregation patterns is less straightforward (Fig. 3A). The spatial segregation analysis gives an *rMSSL* value for both biofilms of around 0.23 ± 0.03 (Table S3). This indicates the average segregation level over all distances is similar in both strains, but as with all averages, the distribution of values comprising the average might be fully different and therefore this does not necessarily mean the two segregation patterns are the same. That this is indeed not the case can be deduced from different *MSSD* and even more from strongly different average slopes of $\widehat{S_d}$ curves (Table S3). Even better insight can be gained by comparing the

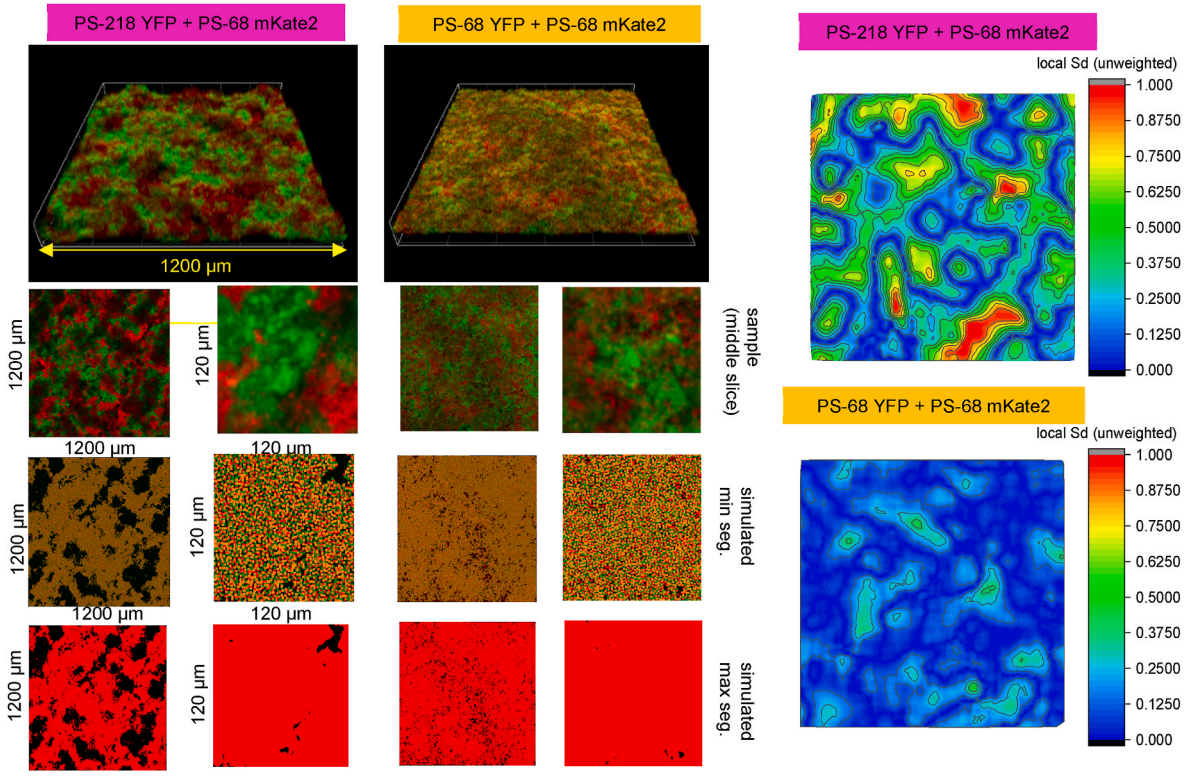

Fig. 3A. Multiscale spatial segregation analysis of two strain biofilms, example 2. 3D reconstructions presented as maximum intensity projections of biofilms formed by two differently labelled bacterial strains based on confocal scanning laser microscopy (CLSM) image slices are shown on top. The green and red color represents *B. subtilis* strain constitutively expressing YFP and mKate fluorescent protein, respectively. 15–25 image slices (forming a CLSM stack of image slices) with optical slice thickness of 14 μm were acquired for each biofilm. The middle image slice in the CLSM image stack representing the FOVs of size (d) of 1200 μm x 1200 is shown together with additional zoom in (120 μm × 120 μm). The corresponding image of simulated minimal and maximal segregation of the two strains in the biofilm is shown. For simulation of maximal segregation, we assumed that only one strain is present in the slice of CLSM stack (in this case the red, mKate strain, but result would be the same for yfp strain). The contour plots show local segregation level S_d at $d = 120$ μm in the space of the middle slice (1200 μm × 1200 μm). (For interpretation of the references to color in this figure legend, the reader is referred to the Web version of this article.)

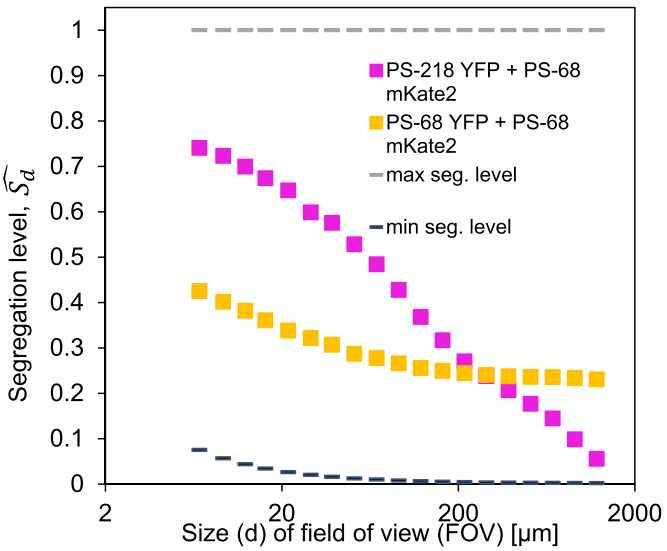

Fig. 3B. The CLSM images of *B. subtilis* biofilms in Fig. 3A were analysed by our algorithm based on eqs (5)–(11) and corresponding segregation levels as a function of size of field of view (FOV) are presented for all bacterial strain combinations. The curves of simulated minimal and maximal segregation cases for the two bacterial strain combinations do not differ significantly, therefore only one max and min segregation curve is presented. The sampling error is within the symbol size. The curves shown represent one of the three replicates shown as averages in Supplementary information of [14].

$\widehat{S_d}$ curves directly (Fig. 3B) where it can be seen why it is important to quantify the segregation level, $\widehat{S_d}$, as a function of size of the FOV and not determine segregation level just at 1 *d*. Although the overall segregation levels (*rMSSL*) of the two compared biofilms are similar, their $\widehat{S_d}$ curves are markedly different (Fig. 3B), indicating that segregation in these biofilms differs significantly and depends on the scale of observation. Comparison of $\widehat{S_d}$ at the FOV of *dmax* (size of the image – 1220 μm in this case) shows that the segregation at this spatial scale in the biofilm PS-68 YFP + PS-68 mKate2 is stronger than in biofilm PS-218 YFP + PS-68 mKate2. A segregation level, $\widehat{S_d}$, of 1 at *dmax* means that in all slices of the particular biofilm, we detect only one strain, whereas 0 indicates that in all slices both strains are present, as expected from their overall amounts in the biofilm. Therefore, a deviation from $\widehat{S_d} = 0$ at *dmax* indicates that in some slices one strain is more dominant than the other. At the intersection of both segregation curves at about a FOV of size $d = 300$ μm, the segregation level in both biofilms is the same ($\widehat{S_d} = 0.25$). This value of $\widehat{S_d}$ indicates that at these spatial scales one of the strains in the biofilm will be slightly dominant over the other (according to eq (6), the two strains would be 1.7 : 1). When going to smaller FOVs, the differences between segregation in the two biofilms become more prominent (Fig. 3B). Inspection of the $\widehat{S_d}$ of biofilms at the FOV size of tens of bacteria (e.g., $d = 20$ μm) indicates that the segregation at this spatial scale is higher in biofilm PS-218 YFP + PS-68 mKate2 compared to PS-68 YFP + PS-68 mKate2. At the smallest observable FOV of size corresponding to a few bacteria (*dmin* = 7 μm), the biofilm PS-218 YFP + PS-68 mKate2 has $\widehat{S_d} = 0.75$, indicating a high segregation level as most FOVs will have high dominance of either PS-218 YFP or PS-68 mKate2 (according to eq (6), the strain ratio is 7 : 1). On the other hand, biofilm PS-68 YFP + PS-68 mKate2 has $\widehat{S_d} = 0.4$, indicating a less prominent dominance of one strain over the other (according to eq (6), the strain ratio is 2.3 : 1). The segregation between the two biofilms can be further investigated by the spatial distribution of local segregation levels, S_d. In the example given in Fig. 3A, S_d at $d =$ 120 μm of the confocal image slice representing the cross-section of the biofilm in the middle of its thickness were plotted on the corresponding contour plots. The variability and the general values in S_d are much higher in the biofilms PS-218 YFP or PS-68 mKate2 compared to the biofilms of PS-68 YFP + PS-68 mKate2, which is in agreement with the assessment that the segregation patterns in the two biofilms differ.

From the above analysis we see that it is possible to quantitatively differentiate segregation levels of strains in biofilms at different scale of observation (i.e., the size of FOV) and that these differences are dependent on the spatial scale of observation.

2.5. Analysis of segregation in well-mixed sonicated biofilm suspensions of two bacterial strains

The biofilms composed of two bacterial strains exhibited clear spatial dependant segregation (Fig. 3B). To further challenge the proposed multiscale spatial segregation approach and show its sensitivity, we disintegrated the two-strain biofilms by sonication and then treated cell suspensions by vortex stirrer to improve the mixing of the two bacterial strains. Both suspensions were inspected by microscopy (Fig. 4A) and the digital images acquired were subjected to multiscale spatial segregation analysis (Fig. 4B and Table S4). The segregation level curves (Fig. 4B) for sonicated biofilms drastically changed compared to intact biofilm segregation curves (Fig. 3B), and became, as expected, closely similar to the minimal segregation level curve (Fig. 4B), indicating improved mixing of the two bacterial strains after sonication. Note that without having the minimal segregation curve, which is the simulated negative control, one could wrongly conclude that the segregation of $\widehat{S_d} = 0.46$ at $d = 13$ μm is significant. The segregation level curve of the strain pair PS-68 YFP + PS-68 mKate2 suspension closely resembled the minimum segregation level curve of complete mixing, while the strain pair PS-218 YFP + PS-68 mKate2 suspension showed a slight deviation from it (Fig. 4B). Accordingly, the *rMSSL* of the strain pair PS-68 YFP + PS-68 mKate2 was 0.005 ± 0.007 and *rMSSL* of the strain pair PS-218 YFP + PS-68 mKate2 was 0.026 ± 0.010, indicating a significant difference. This was confirmed by calculating a *t*-test for $\widehat{S_d}$ of the FOV with *d* from 30 to 1000 μm ($p < 0.03$ for all $\widehat{S_d}$), where the difference with $\widehat{S_d^{min}}$ was most pronounced (Fig. 4B). This indicates that the cells of the disintegrated PS-218 YFP + PS-68 mKate2 biofilm are not entirely mixed, as one would expect. A possible explanation is that some cells of the biofilm of strain pair PS-218 YFP + PS-68 mKate2 remained physically connected (via exopolymers, for example) after sonication. The largest *d* with the segregation level, $\widehat{S_d}$, that significantly differs from S_d^{min} (the segregation level in randomly mixed sample) was approximately at $d =$ 1000 μm. Therefore, the maximal length of the physical connections preventing perfect mixing corresponds to $d = 1000$ μm. Note that this is the largest *d* from the analysed points, where $\widehat{S_d}$ can be different than 0; $\widehat{S_d}$ at *dmax,* which is 1280 μm in this case, will be in 2D images always 0, because from the FOV of size of *dmax* the overall strain abundances are obtained and therefore $a = A$ and $b = B$, yielding $\widehat{S_d} = 0$ in eq (3). Therefore, it is possible that if we had acquired the microscopy image with even larger FOV (*dmax* > 1280 μm) the $\widehat{S_d} > \widehat{S_d^{min}}$ would hold even for $d > 1000$ μm. As intercellular connections likely prevented maximal mixing, it can be concluded that harsher sonication conditions should have been used to fully disintegrate the PS-218 YFP + PS-68 mKate2 biofilm.

The results of the proposed *MSSegregation* analysis approach agrees with predicted drop in segregation in disintegrated vs. native two-strain biofilms. Also, small differences in segregation level in well-mixed cultures that are otherwise difficult to spot can be detected by this approach. A possible misinterpretation can be avoided by comparing obtained segregation levels to segregation extremes in controls.

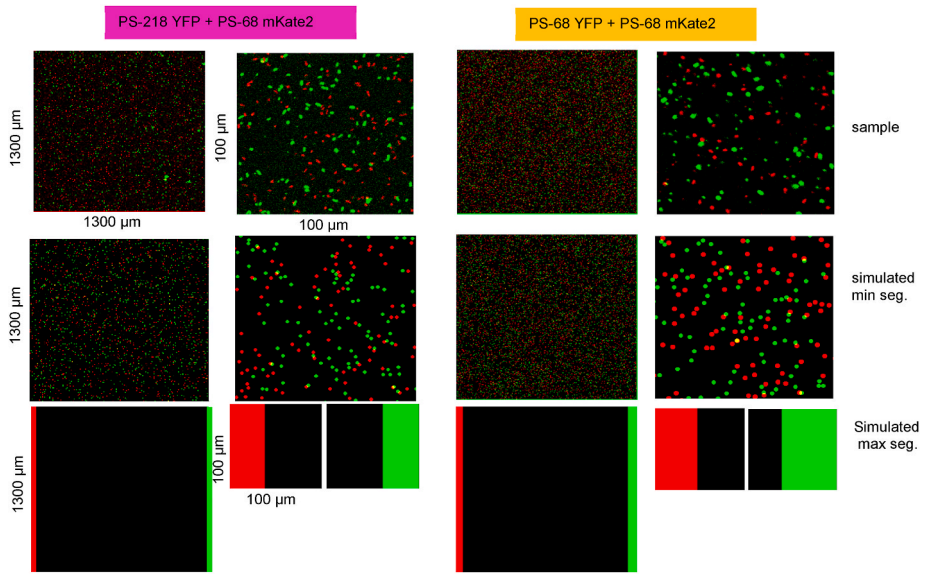

Fig. 4A. Multiscale spatial segregation analysis of biofilms of two *B. subtilis* strains that were disintegrated to individual bacterial cells by sonication; the sonicated samples were imaged by confocal scanning laser microscopy (CLSM); two sets of images presenting two strain mixtures are shown; the microscope images of samples are presented as full size images of 1300 µm × 1300 µm and zoom-in images of 100 µm × 100 µm; the corresponding images of simulated minimal and maximal segregation of the two bacterial strains in the biofilm is shown. The slice optical thickness in the microscopy hardware and sample thickness exceeded the size of two individual cells thereby permitting individual cells to overlap (yellow). Therefore, for simulation of minimal segregation, overlapping of individual cells was allowed. For simulation of maximal segregation, we assumed that strains cannot exclude each other out of the image. (For interpretation of the references to color in this figure legend, the reader is referred to the Web version of this article.)

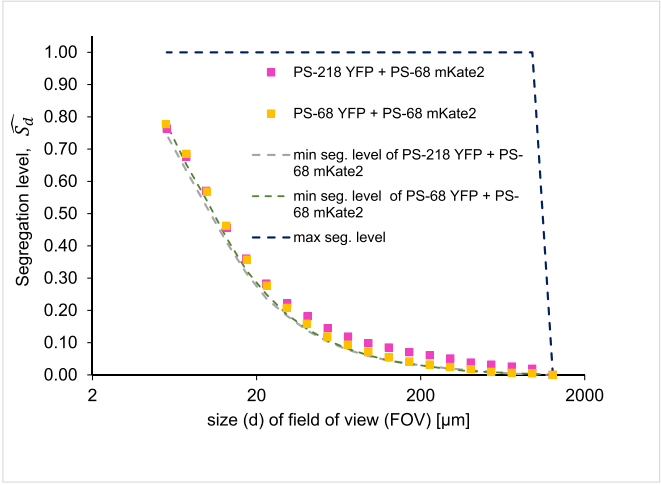

Fig. 4B. The CLSM images of disintegrated biofilms of two *B. subtilis* strains to individual bacterial cells and corresponding simulated segregations in Figure 4A were analysed by our algorithm (eqs (5)–(11)). Corresponding segregation levels as a function of size of field of view (FOV) are presented for the two bacterial strain combinations. The sampling error is within the symbol size.

2.6. Time-efficiency of multiscale spatial segregation analysis

The time taken on the AMD F6 (3.2 GHz)-based PC (2012 build), using a single core CPU to obtain segregation level of biofilm microscopy images, was about 6 min for an 18 slice-CLSM stack. To simulate corresponding segregation extreme images and calculate their segregation level curves (segregation extreme curves) took 13 min. Although one can run parallel instances of FIJI-ImageJ and use the multi-core abilities of most modern computer processors in order to process several stacks of images in parallel, the question arises, if the introduction of new segregation metrics slowed down the analysis process and would have not been better to find a way to improve and build our *MSSegregation* approach around existing van Gestel approach (eq (1)). To clarify this, we benchmarked the cores (i.e. eq (1) and eq (5)) of the two approaches on the same biofilm images (one slice of the CLSM stack in Fig. 3A) by calculating segregation levels at two different d (Fig. 5). In general the values of the two measures correlated well, although the relative differences increased with d (Table S5). However, at the smaller d our approach is more than two times faster and at the larger d for more than 30 times faster. Note that in the Van Gestel approach the circle of dimeter d is placed on random focal cells, therefore the list of foreground pixels (representing the cells) with respective x and y coordinates is needed as a first step in application of Van Gestel approach. Because we believe that imageJ is not very time efficient in extracting these coordinates from the image and other more efficient approaches exist, we did not include the time taken for this extraction in benchmarking of Van Gestel approach. Nevertheless, the differences shown in Fig. 5, would have been even greater if the time taken for conversion of foreground pixels to x and y coordinates was taken into account.

3. Discussion

The new approach to the analysis of the multiscale spatial segregation in digital images was successfully tested on synthetic and real digital images of binary mixtures. Also, the synthetic chessboard images, where classical segregation measures such as the Duncan Index of dissimilarity [22] fail to distinguish different degrees of segregation present [23], were successfully analysed by the new approach. When analysing complex biological mixtures, such as two species biofilms, the multiscale spatial segregation can reveal and quantify the degree of segregation and give information on how segregation correlates with the scale of observation. It is known that bacteria can interfere with each other either through physical displacement or actively, by interference competition [24], applying mechanisms such as cell contact inhibition [24–26], diffusible extracellular toxins [27] or signals [28]. All these phenomena can span the spatial scale from micrometres to centimetres [29]. In such cases, the multiscale spatial segregation analysis is very useful, as one can distinguish between different segregation levels at

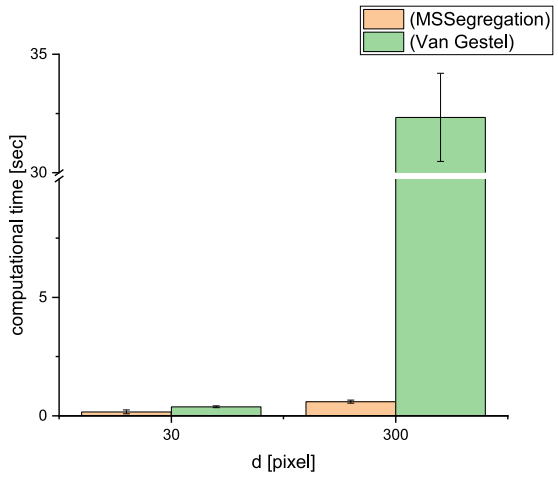

Fig. 5. Computational time required to calculate segregation level in biofilm microscopy image (1946 × 1946) using *MSSegregation* algorithm (eq (5)) or algorithm described by Van Gestel et al., 2015 (eq (1)); d is the size of the square field of view (FOV) (MSSegregation) or diameter of the circle (Van Gestel). In *MSSsegration*, the local segregation level (of two particles, e.g. two bacterial strains, 1 and 2) is calculated in each FOV that is randomly placed over the image, the average of local segregation levels presents segregation level at certain d; in Van Gestel method the segregation level is defined as the difference of average relative frequencies of the strain 1 around the focal cell of strain 2 and the average of relative frequencies of the strain 1 around the focal cell of strain 2 calculated within the circles of diameter d placed over random focal cells. The n, number of surveyed FOV or circles was adjusted to obtain segregation levels with the same coefficients of variations (at $d = 30$ pixel CV = 1%, n(MSSegregation) = 5000, n(Van Gestel) = 5000; at $d = 300$ pixel, CV = 1.5%, n(MSSegregation) = 2000, n(Van Gestel) = 10000).

different spatial scales and also quantify them. By introducing multiscale spatial segregation level (*MSSL*) we were able to express the spatial scale dependant segregation in an image by a single number. We have shown that (simulated) positive and negative controls for segregation extremes are important for proper interpretation and included them quantitatively in the relative multiscale spatial segregation level (*rMSSL*). These concepts were not present in previous advanced approaches for studying segregation in biofilms [17,18,21].

Our approach has a number of advantages. The segregation level of each subspace (i.e. FOV) in an image can be directly assessed and compared to what an observer sees. From the segregation level, one can deduce the ratio of the two strains in the FOV (eq (6)) aiding the interpretation. Furthermore, one can obtain a distribution of segregation levels across the image. All of these is not possible, when applying the method by van Gestel (eq (1)), because the focal cells of the respective strains are randomly and independently selected across the whole image. In this process the local spatial correlation among strain 1 and strain 2 is lost. This is also likely the reason why at larger d the number of evaluated subspaces (FOVs or circles) to obtain the same coefficient of variation is significantly smaller in our approach compared to van Gestel approach. The latter approach is additionally slowed down by using circles, which are computationally more demanding than square shaped FOVs.

Currently, our approach is limited to the segregation analysis of only two components (e.g. biofilms of two species), which means that several species biofilms, as often found in nature, cannot be analysed by it. However, in the future, it might be possible to extend the approach to more species. For example, adding a third species, means that the segregation can now exist between three different pairs of species. Accordingly, the eq (3) can then be adopted to take into account all three species pairs.

We have derived quantitative and easy-to-interpret measures for the multiscale spatial segregation analysis of digital images and implemented them into an easily applicable algorithm that solves the drawbacks of existing approaches for segregation analysis in biofilms. The algorithm, implemented in freely available software, calculates the segregation levels of two components in a digital image as a function of the spatial scale of observation (i.e., size of field of view). Based on the images analysed, the algorithm also simulates maximal and minimal segregation cases that present negative and positive controls in our analysis, which further improves the objectiveness of the proposed scientific approach and prevents possible misinterpretations. The application of the multiscale spatial segregation analysis is not restricted to the examples presented: mixed species biofilms, bacterial suspensions or oats and raisins mixtures. It can be applied whenever the quantification of segregation level or mixing efficiency of two components is required and digital images of such a binary system can be obtained.

4. Methods

4.1. Macro implementation

The algorithm to calculate different segregation measures (eq (1) to eq (11)) was implemented in ImageJ macro language using the ImageJ (FIJI) environment [30,31], which is an open-source microscopy image processing software. It has multiple built-in functionalities and, most importantly, it is compatible with the majority of microscopy data output formats thanks to the BioFormats plug-in Ref. [32]. Our analysis is performed by custom macros (Fig. S2), comprising the macro package *MSSegregation* (see Supplementary, SI Methods, Macro implementation and see user manual for details and examples available at https://github.com/IztokD/MSSegregation-package).

4.2. Acquisition of example images and macro settings

4.2.1. Synthetic images for testing

The maximum segregation images (Fig. 1) and chessboard images were drawn in ImageJ (FIJI) environment. The settings for macro package *MSSegregation* are given in Supplementary information (SI Methods, Acquisition of example images and macro settings).

4.2.2. Biofilms of two bacterial strains

The biofilms containing two bacterial strains each constitutively expressing fluorescent proteins (green – YFP; red – mKate2; Fig. 3A, Table S6) were grown in 30-mm, glass-bottom petri dishes. After overnight incubation, when the biofilm in the form of a pellicle floating on the interface air/growth medium was mature, the growth medium was removed by syringe. The fluorescence images of the biofilms were acquired by inverted confocal laser scanning microscopy Axiovsion Z1, LSM800 (Zeiss, Germany), using EC Plan-Neofluar 10x/0.30 Ph 1 objective and two laser channels: a 488 nm laser to acquire green fluorescence and a 561 nm laser to acquire red fluorescence. The pinhole size for the green channel was set to 1.0 AU and the red channel to 1.2 AU. The frame time was 3.7 s, averaging was set to 4 and 930 × 930-pixel single frame size. The mosaic function of Zen 2.3 (Zeiss, Germany) was used for 2 × 2 frame acquisition. The stitched image of 1960 × 1960 pixels covered a FOV of size 1.2 mm × 1.2 mm. Slicing was set to half of the Nyquist distance, which was 6 μm.

To improve quality and resolution, the confocal laser scanning microscopy images were single pixel filtered and deconvolved using the Tikhonov-Miller algorithm applied in DeconvolutionLab2 application [33], with artificial point spread function as obtained by point spread function (PSF) generator application [34], both running in FIJI-ImageJ environment [31]. Images were then thresholded by the following procedure: we applied the ImageJ Li thresholding algorithm [35] and then checked if the thresholding was appropriate. In some instances manual correction was needed as not all the bacteria in the stack were above the suggested threshold. It should be noted that there is no

universal threshold approach that will give in all cases optimal result [36] and that the choice of particular threshold method can influence, as with many other microscopy image analysis, the output of the method [37]. Although the segregation level as calculated by eq (3) has same tolerance against over or under estimation of the particle areas (if a and A or b and B are both equally inflated, the $\widehat{S_d}$ does not change), larger deviations can still impact the $\widehat{S_d}$. For example, by setting the threshold too high, one can artificially create more empty space increasing the likelihood that only one type of the particle will be present in FOV, which increases the calculated segregation levels. Therefore, it is advisable that the users follow the same chosen threshold and denoising protocol throughout their data analysis in order to keep the possible systematic error constant within the experiment and assure valid relative comparisons among biofilms.

The thresholded images of both bacterial strains comprising the same biofilm were converted into a binary format (pixel value of 255 means the pixel belongs to particular strain, 0 it belongs to empty space or to the other strain), which served as an input for *Sim_seg_extremes* and *MSS_calc* macros. The *dmin* corresponded to half of the optical slice thickness of original (no deconvolution) images (≈6 μm) and *dmax* to 1.2 mm.

For multiscale spatial segregation analysis, the sampling factor in macro *MSS_calc* was set to 0.005 (default value), enabling the evaluation of around 10,000 randomly placed FOVs at *dmin* The standard error of the segregation level was at all sizes of FOV <2%. The resolution factor was set to 0.75 (default value), giving a range of 22 points on a graph of segregation level vs. size (d) of FOV. For simulation of the minimal segregation, the bacterial cell was assumed to be a circle 1.8 μm in diameter, which corresponded well to the sizes determined in the sonicated samples, from which we could resolve the size of the individual cells (Fig. 3B). The simulated cells were randomly distributed in the biofilm of the same shape as original, and overlap was allowed. For maximal segregation case, it was assumed that in each image slice only one strain was present and that shape of the original biofilm was preserved.

4.2.3. Sonicated biofilms suspensions of two bacterial strains

The two-strain biofilms were harvested from a growth medium and transferred to Eppendorf tubes, where they were sonicated with an MSE 150 Watt Ultrasonic Disintegrator Mk2 equipped with exponential probe for 5 s at an amplitude of 15 μm. The slides of the bacterial suspension obtained were then observed under inverted confocal laser scanning microscopy.

The slides of sonicated bacterial biofilms were observed using an Axiovsion Z1, LSM800 microscope (Zeiss, Germany), with a LD Plan-Neofluar 20x/0.4 Korr M27 objective and two laser channels – a 488 nm laser to acquire green fluorescence and a 561 nm laser to acquire red fluorescence. The pinhole size for green channel was set to 1.0 AU and the red channel to 1.2 AU. Frame time was 3.7 s, averaging was set to 4 and a 948 × 948-pixel frame size was set. The mosaic function of Zen 2.3 (Zeiss, Germany) was used for 4 × 4 frame acquisition. The stitched image of 3972 × 3972 pixels covered a FOV of sizes 1.2 mm × 1.2 mm. The total number of bacteria was >12,000. A single optical slice was recorded.

For multiscale spatial segregation analysis, the sampling factor in macro *MSS_calc* was set to 0.005 (default value), which means that around 10,000 randomly placed FOVs were evaluated at *dmin*. The standard error of the segregation level was at all sizes of FOV <2%. The resolution factor that determines the spacing among FOV sizes for which segregation level is calculated was set to 0.75 (default value).

For simulation of the minimal segregation, the cells were assumed to be circles with diameters representing the average diameter obtained from the statistical analysis of all cells in the image. In the combination of PS-218 YFP and PS-68 mKate2, both strains had a circle diameter of 1.8 μm; in the case of the combination PS-68 YFP and PS-68 mKate2, the cell circle diameter was 2.2 μm and 2.5 μm, respectively. As the specimen thickness and optical slice thickness were bigger than 2 x cell diameter, the overlapping of cells was allowed in the simulation of minimal segregation. For maximal segregation simulation, the presence of both strains in the same image was assumed.

Data and code availability

The multiscale spatial segregation analysis approach is implemented in ImageJ macro language and consists of four macros that comprise *MSSegregation* package. The package including the manual is freely available under the terms of Modified BSD License at https://github.com/IztokD/MSSegregation-package. It can be run in open source Fiji-ImageJ application available online https://imagej.net/Fiji. The original (source) images used to perform analysis in this article are available at https://github.com/IztokD/MSSegregation-package.

CRediT authorship contribution statement

Iztok Dogsa: Conceptualization, Software, Validation, Formal analysis, Investigation, Resources, Writing – original draft, Writing – review & editing, Supervision. **Ines Mandic-Mulec:** Methodology, Data curation, Funding acquisition, Supervision.

Declaration of competing interest

The authors declare the following financial interests/personal relationships which may be considered as potential competing interests: co-author, Ines Mandic-Mules is serving as Editorial board member in Biofilms.

Data availability

The data is freely available in public domain github: https://github.com/IztokD/MSSegregation-package

Acknowledgements

We thank Tjasa Stosicki for growing and disintegrating the mixed species biofilms. We also thank dr. Anna Dragoš for the valuable comments to improve the clearness and readability of the manuscript. This work was supported by the Slovenian Research And Innovation Agency (ARIS) national program grant P4-0116, ARIS research grants [J4-1775, J1-3021, J4-9302, J4-4550]. The microscopic analysis was supported by funding from ARIS to Infrastructural Centre Microscopy of Biological Samples (MRIC UL, I0-0022-0481-08), at Biotechnical Faculty, University of Ljubljana, Slovenia.

Appendix A. Supplementary data

Supplementary data to this article can be found online at https://doi.org/10.1016/j.bioflm.2023.100157.

References

[1] Shigesada N, Kawasaki K, Taramoto E. Spatial segregation of interacting species. J Theor Biol 1979;79:83–99.
[2] Vos M, Wolf AB, Jennings SJ, Kowalchuk GA. Micro-scale determinants of bacterial diversity in soil. FEMS (Fed Eur Microbiol Soc) Microbiol Rev 2013;37:936–54.
[3] Kovács Á. Impact of spatial distribution on the development of mutualism in microbes. Front Microbiol 2014;5:649.
[4] Cordero OX, Datta MS. Microbial interactions and community assembly at microscales. Curr Opin Microbiol 2016;31:227–34.
[5] Welch JLM, Rossetti BJ, Rieken CW, Dewhirst FE, Borisy GG. Biogeography of a microbiome at micron scale. Proc Natl Acad Sci USA 2016;113:E791–800.
[6] Lyons NA, Kraigher B, Stefanič P, Mandić-Mulec I, Kolter R. A combinatorial kin discrimination system in Bacillus subtilis. Curr Biol 2016;26:733–42.

[7] Dragoš A, Kiesewalter H, Martin M, Hsu CY, Hartmann R, Wechsler T, Eriksen C, Brix S, Drescher K, Stanley-Wall N, Kümmerli R, Kovács ÁT. Division of labor during biofilm matrix production. Curr Biol 2018;28:1903–13.
[8] Cai P, Sun X, Wu Y, et al. Soil biofilms: microbial interactions, challenges, and advanced techniques for ex-situ characterization. Soil Ecol. Lett. 2019;1:85–93.
[9] Stefanic P, Kraigher B, Lyons NA, Kolter R, Mandice-Mulec I. Kin discrimination between sympatric Bacillus subtilis isolates. Proc Natl Acad Sci USA 2015;112:14042–7.
[10] Waithe D, Brown JM, Reglinski K, Diez-Sevilla I, Roberts D, Eggeling C. Object detection networks and augmented reality for cellular detection in fluorescence microscopy. J Cell Biol 2020;219:e201903166.
[11] Hartmann R, Jeckel H, Jelli E, et al. Quantitative image analysis of microbial communities with BiofilmQ. Nat Microbiol 2021;6:151–6.
[12] Heydorn A, et al. Quantification of biofilm structures by the novel computer program COMSTAT. Microbiology 2000;146:2395–407.
[13] Sharma A, Wood KB. Spatial segregation and cooperation in radially expanding microbial colonies under antibiotic stress. ISME J 2021;15:3019–33.
[14] Bolješić M, Kraigher B, Dogsa I, Jerič Kokelj B. Mandic-mulec, I. Kin discrimination modifies strain distribution, spatial segregation, and incorporation of extracellular matrix polysaccharide mutants of Bacillus subtilis strains into mixed floating biofilms. Appl Environ Microbiol 2022;88:e0087122.
[15] Momeni B, Brileya KA, Fields MW, Shou W. Strong inter-population cooperation leads to partner intermixing in microbial communities eLife, vol. 2; 2013, e00230.
[16] Goldschmidt F, Regoes R, Johnson D. Successive range expansion promotes diversity and accelerates evolution in spatially structured microbial populations. ISME J 2017;11:2112–23.
[17] Mitri S, Xavier JB, Foster KR. Social evolution in multispecies biofilms. Proc Natl Acad Sci USA 2011;108:10839–46.
[18] Nadell CD, Foster KR, Xavier JB. Emergence of spatial structure in cell groups and the evolution of cooperation. PLoS Comput Biol 2010;6:e1000716.
[19] Krajnc M, Stefanic P, Kostanjšek R, Mandic-Mulec I, Dogsa I, Stopar D. Systems view of Bacillus subtilis pellicle development. NPJ Biofilms Microbiomes 2022;8:25.
[20] Wilking JN, Zaburdaev V, De Volder M, Losick R, Brenner MP, Weitz DA. Liquid transport facilitated by channels in Bacillus subtilis biofilms. Proc Natl Acad Sci USA 2013;110:848–52.
[21] van Gestel J, Weissing FJ, Kuipers OP, Kovács AT. Density of founder cells affects spatial pattern formation and cooperation in Bacillus subtilis biofilms. ISME J 2014;8:2069–79.
[22] Duncan OD, Duncan B. A methodological analysis of segregation indices. Am Socio Rev 1955;20:210–7.
[23] Harris R, Owen D. Implementing a Multilevel Index of Dissimilarity in R with a case study of the changing scales of residential ethnic segregation in England and Wales. Environ Plan B Urban Anal City Sci 2018;45:1003–21.
[24] Nadell CD, Drescher K, Foster KR. Spatial structure, cooperation and competition in biofilms. Nat Rev Microbiol 2016;14:589–600.
[25] Aoki SK, Diner EJ, de Roodenbeke CT, et al. A widespread family of polymorphic contact-dependent toxin delivery systems in bacteria. Nature 2010;468:439–42.
[26] Hood RD, Singh P, Hsu FS, et al. A type VI secretion system of Pseudomonas aeruginosa targets a toxin to bacteria. Cell Host Microbe 2010;7:25–37.
[27] Hernandez-Valdes JA, Zhou L, de Vries MP, Kuipers OP. Impact of spatial proximity on territoriality among human skin bacteria. NPJ biofilms and microbiomes 2020;6:30.
[28] Stubbendieck RM, Straight PD. Multifaceted interfaces of bacterial competition. J Bacteriol 2016;198:2145–55.
[29] Stubbendieck RM, Vargas-Bautista C, Straight PD. Bacterial communities: interactions to scale. Front Microbiol 2016;7:1234–53.
[30] Rueden CT, Schindelin J, Hiner MC, DeZonia BE, Walter AE, Arena ET, Eliceiri KW. ImageJ2: ImageJ for the next generation of scientific image data. BMC Bioinf 2017;18:529.
[31] Schindelin J, et al. Fiji: an open-source platform for biological-image analysis. Nat Methods 2012;9:676–82.
[32] Linkert M, Rueden CT, Allan C, Burel J-M, Moore W, Patterson A, Swedlow JR. Metadata matters: access to image data in the real world. JCB (J Cell Biol) 2010;189:777–82. 18.
[33] Sage D, et al. DeconvolutionLab2: an open-source software for deconvolution microscopy. Methods 2017;115:28–41.
[34] Kirshner H, Aguet F, Sage D, Unser M. 3-D PSF fitting for fluorescence microscopy: implementation and localization application. J Microsc 2013;249:13–25.
[35] Li CH, Tam PKS. An iterative algorithm for minimum cross entropy thresholding. Pattern Recogn Lett 1998;19:771–6.
[36] Sankur B. Survey over image thresholding techniques and quantitative performance evaluation. J Electron Imag 2004;13:146–65.
[37] Luo TL, Eisenberg MC, Hayashi MAL, et al. A sensitive thresholding method for confocal laser scanning microscope image stacks of microbial biofilms. Sci Rep 2018;8:13013.